



Cite this: DOI: 10.1039/d6tc00480f

# Through-space cation- $\pi$ quadrupole-monopole design enables selective suppression of third-order nonlinear optical Kerr effects

Daniels Jelisejevs,<sup>a</sup> Arturs Bundulis,<sup>b</sup> Anete Sapne<sup>b</sup> and Kaspars Leduskrasts<sup>b</sup> \*<sup>a</sup>

Organic materials capable of exhibiting high-order nonlinear optical responses are central to the advancement of photonic technologies. However, the molecular-level mechanisms that govern selective control over nonlinear optical response-order remain limited. Here, we employ a quadrupole-monopole design strategy based on intramolecular through-space cation- $\pi$  interaction to uncover a new principle for tuning nonlinear optical behavior in purely organic systems. A series of  $\pi^+$ - $\pi$  conjugates were synthesized and systematically analyzed using Z-scan measurements. We demonstrate that intramolecular quadrupole-monopole coupling selectively suppresses the third-order Kerr effect, while enabling a pure fifth-order nonlinear optical response. The magnitude of the fifth-order response correlates with the electrostatic interaction strength between the  $\pi$  and  $\pi^+$  centers, following a  $1/R^4$  dependence characteristic of monopole-induced dipole polarization. These findings establish electrostatic through-space coupling as a general design principle for inverting the optical nonlinearity hierarchy in organic materials.

Received 12th February 2026,  
Accepted 15th April 2026

DOI: 10.1039/d6tc00480f

rsc.li/materials-c

## Introduction

Materials with strong nonlinear optical (NLO) responses are essential for a wide range of applications, including optical data processing,<sup>1</sup> bioimaging,<sup>2</sup> and photonic devices,<sup>3</sup> enabling advanced functionalities in high-speed data transfer,<sup>4</sup> optical frequency conversion,<sup>5</sup> deep tissue imaging,<sup>6</sup> dynamic holography,<sup>7</sup> laser technologies,<sup>8</sup> telecommunications,<sup>9</sup> and photonic quantum systems.<sup>10</sup> Purely organic NLO materials (PONLOMs) incorporating extended  $\pi$ -systems are particularly advantageous compared to their inorganic counterparts due to their superior NLO susceptibilities,<sup>11</sup> greater structural flexibility, lower production costs, and ability to exhibit NLO effects as isolated molecules in diverse media, such as solvents and polymers.<sup>12</sup> The NLO properties of PONLOMs typically arise from the intramolecular through-bond charge transfer mechanism in a quadrupolar (QP) system.<sup>13</sup>

The QP ( $\pi$ -(hetero)aromatic) nature of PONLOMs is a key aspect enabling nonlinear interaction with light. The donor-acceptor design of PONLOMs can be categorized in non-centrosymmetric QP (I), centrosymmetric QP (II), and through-space QP-QP (III) systems (Fig. 1). While type I PONLOMs show strong second and third order NLO responses,<sup>14</sup>

upon crystallization the centrosymmetric nature of many crystal lattices generates type II systems that eliminate even-order (second, fourth, *etc.*) NLO contributions,<sup>15</sup> maintaining only odd-order NLO responses. Type III systems, where QP units

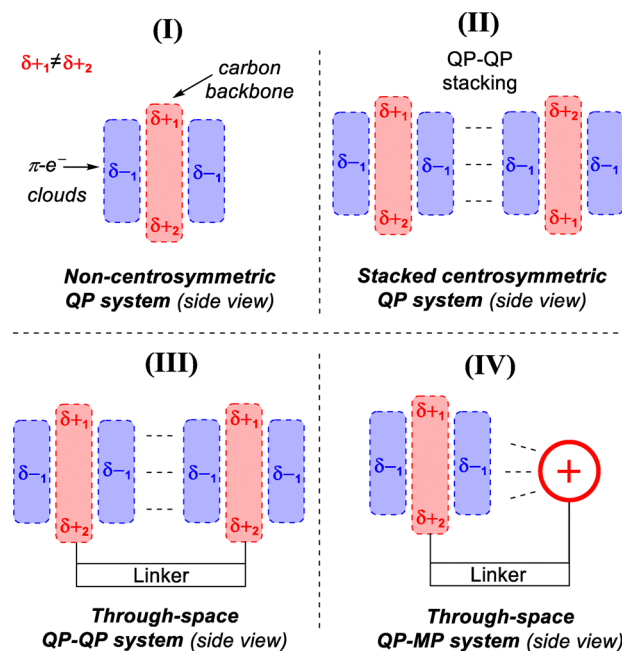


Fig. 1 Previously utilized I–III, and the developed IV QP–MP PONLOM designs.

<sup>a</sup>Latvian Institute of Organic Synthesis, Aizkraukles 21, LV-1006, Riga, Latvia.  
E-mail: kledus@osi.lv

<sup>b</sup>Institute of Solid State Physics, University of Latvia, Kengaraga 8, LV-1063, Riga, Latvia



interact through space,<sup>16</sup> show potential for materials with highly polarizable excited states, improved transparency and stability,<sup>17,18</sup> and support both centrosymmetric and non-centrosymmetric architectures. However, since the 1990s, PONLOMs with type III designs have generally exhibited modest NLO responses<sup>15b,19</sup> and have yet to deliver major breakthroughs in performance. Critically, these type I–III molecular designs rely solely on neutral QP electronic distributions, which fundamentally govern NLO light-matter interactions.<sup>20</sup>

We hypothesized that introducing a monopole (MP) component in a PONLOM design, through the incorporation of a heteroaromatic cation ( $\pi^+$ ) system, could disrupt the established NLO response hierarchy. Cationic  $\pi^+$  systems exhibit strong MP character and facilitate efficient through-space charge transfer (CT).<sup>21–23</sup> Specifically, the strong electrostatic and induction forces of a  $\pi^+$ -system (MP)<sup>24</sup> in a proper architecture could interact with a neutral  $\pi$ -system (QP) to create a novel type IV QP–MP design (Fig. 1). Unlike the neutral  $\pi$ – $\pi$  interactions of type III designs, the intramolecular QP–MP design introduces a permanent electric field component that

fundamentally alters the molecular polarization and breaks the symmetry.

In this work, we demonstrate that intramolecular QP–MP interactions (type IV design) enable selective suppression of the third-order refractive nonlinearity (Kerr effect) while directly accessing fifth-order NLO refraction. The resulting fifth-order response is approximately three orders of magnitude stronger than that of standard benchmark materials such as  $\text{CS}_2$ <sup>25</sup> and is observed in the 800–900 nm range with negligible NLO losses, a spectral window particularly well-suited for telecommunication applications. Hence, the developed QP–MP design represents a paradigm shift from conventional donor–acceptor architectures, establishing multipole tailoring as an effective tool for engineering high-order optical nonlinearities.

## Results and discussion

To investigate the role that QP–MP interactions have on NLO properties, a series of organic compounds 1–6 (Fig. 2) were designed and synthesized. Salts 1a–c, incorporating

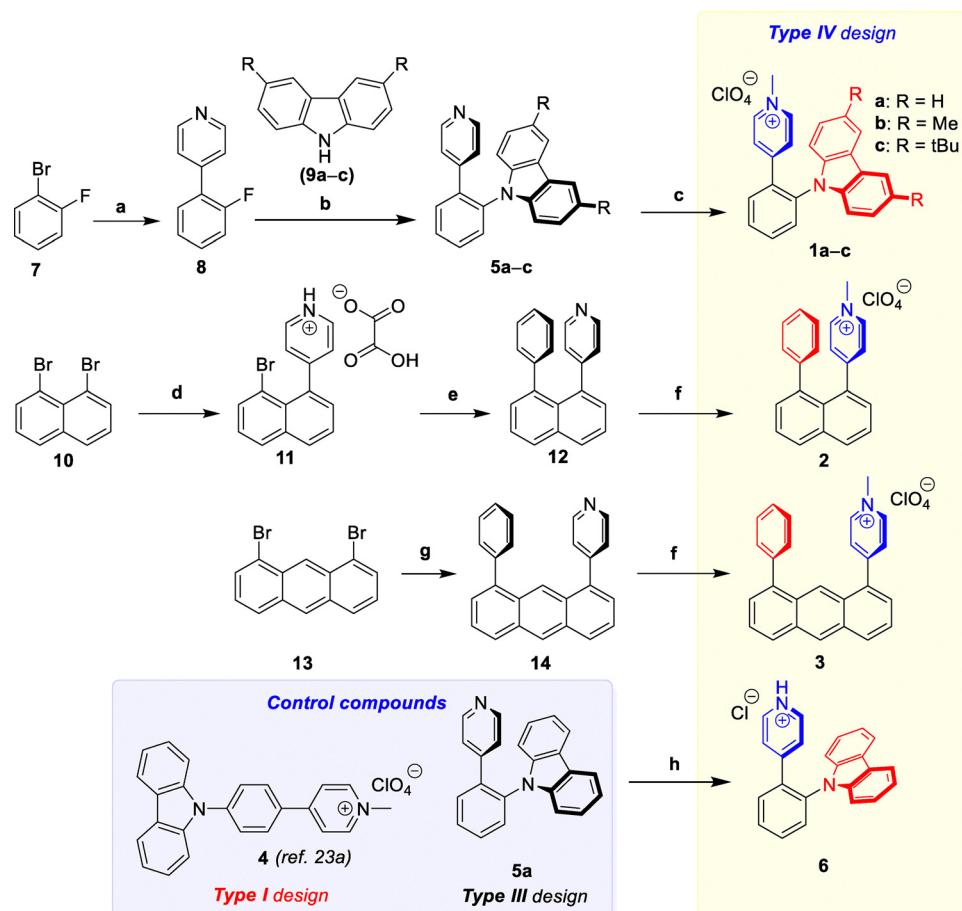


**Fig. 2** Synthesis of compounds with type IV (1–3, 6), type I (4) and type III (5a) designs. Reagents and conditions: (a) pyridine-4-boronic acid hydrate, Pd(dppf)Cl<sub>2</sub>-DCM (5 mol%), K<sub>2</sub>CO<sub>3</sub>, 1:6 water–MeCN, 90 °C, 4 h, 97% (8). (b) KOH, DMSO, 100 °C, 72 h, 48% (5a), 40% (5b), 36% (5c). (c) First MeI, MeCN, 40 °C, 72 h, then AgClO<sub>4</sub>, MeCN, rt, 1 h, 72% (1a), 62% (1b), 67% (1c). (d) First pyridine-4-boronic acid hydrate, Pd(dppf)Cl<sub>2</sub>-DCM (5 mol%), K<sub>2</sub>CO<sub>3</sub>, 1:3 water–MeCN, 90 °C, 2 h, then oxalic acid, rt, 65% (11). (e) Phenyl boronic acid, Pd(dppf)Cl<sub>2</sub>-DCM (5 mol%), K<sub>2</sub>CO<sub>3</sub>, 1:4 water–MeCN, 90 °C, 2 h, 62% (12). (f) First MeI, MeCN, 70 °C, 2 h, then AgClO<sub>4</sub>, MeCN, rt, 1 h, 81% (2), 76% (3). (g) Pyridine-4-boronic acid hydrate, phenyl boronic acid, Pd(dppf)Cl<sub>2</sub>-DCM (10 mol%), K<sub>2</sub>CO<sub>3</sub>, 1:10 water–PhMe, 90 °C, 36 h, 41% (14). (h) HCl, MeCN, rt (6).



$\pi^+$  (*N*-methylpyridinium) and  $\pi$  (carbazole or functionalized carbazole) units at the 1- and 2-positions of a benzene ring, were synthesized starting from commercially available 1-bromo-2-fluorobenzene **7**. A Pd-catalyzed Suzuki coupling with pyridine boronic acid afforded fluoride **8**, which subsequently underwent  $S_NAr$  substitution with carbazoles **9a–c** to yield compounds **5a–c**. Subsequent *N*-alkylation with MeI, followed by counterion metathesis, afforded the corresponding pyridinium ( $Py^+$ ) perchlorates **1a–c**. To broaden the structural scope, a naphthalene-linked salt **2** was synthesized from dibromide **10** utilizing sequential Suzuki couplings. Initial coupling with pyridine boronic acid produced bromide **11**, which upon further coupling with phenyl boronic acid yielded pyridine **12**. Conversion of free base **12** to  $Py^+$  salt **2** was achieved under conditions analogous to those used for **1a–c**. The anthracene-linked compound **3** was prepared from dibromide **13** through a one-pot Suzuki reaction with pyridine and phenyl boronic acids to afford pyridine **14**, which was subsequently *N*-alkylated and subjected to anion exchange to give  $Py^+$  perchlorate **3**. To control for the presence of intramolecular QP–MP interactions in compounds **1–3**, a linear isomer of **1**, compound **4**, was synthesized according to a previously reported protocol.<sup>23a</sup> In addition, evaluation of **5a**, along with its protonated derivative **6**, provided further insight into the role of the intramolecular QP–MP interaction design. Complete characterization of all novel compounds was achieved using  $^1H$  and  $^{13}C$  NMR, IR spectroscopy, HRMS, elemental analysis, and melting point measurements, as appropriate (see Pages S3–S9, SI).

The absorption of compounds **1–6** was examined in MeCN at *ca.*  $10^{-5}$  M concentration under ambient conditions (see Fig. S1–S5, SI). The  $Py^+$  salts **1a–c** exhibited three absorption peaks in the 238–245 nm, 276–298 nm, and 317–349 nm

regions, alongside a broad, low-intensity CT band spanning 365–435 nm. The naphthalene-derivative **2** displayed absorption bands at 235 nm, 259 nm, and 287 nm, accompanied by a broad CT band from 327 to 425 nm. In contrast, salt **3** showed two distinct absorption bands, one at 250 nm and a moderately intense, broad CT peak extending from 325 to 460 nm. Compound **4** (isomer of **1a**) absorption peaks were observed at 237 nm, 258 nm, and 281 nm, including a significant CT band in the 320–440 nm region. The free base pyridine **5a** showed absorption at 247 nm, 292 nm, 324 nm, and 338 nm. The protonated counterpart **6** displayed absorption bands at 239 nm, 287 nm, 320 nm, and 333 nm, but also a weak CT absorption band in the 350–437 nm region. Thus, all synthesized  $Py^+$  salts exhibited broad CT absorption bands, which in type **IV** designs (**1–3** and **6**) are attributed to the intramolecular through space CT between the red  $\pi$  and  $Py^+$  system (Fig. 2).

The intramolecular through space CT in compounds **1–3** and **6** was corroborated by quantum chemical calculations. Accordingly, the optimized ground-state geometries of compounds **1–6** were calculated using Gaussian 09 at the B3LYP/6-31+G(d) level of theory (Fig. 3). Compounds **1a–c** and **6** adopt conformations that support intramolecular cation– $\pi$  interactions between the  $Py^+$  unit and the nearest  $\pi$ -system. In these molecules, the interaction geometry is angled, with centroid–centroid distances ( $R_{cc}$ ) of 4.61, 4.59, 4.62, and 4.58 Å for **1a**, **1b**, **1c**, and **6**, respectively. In contrast, the naphthalene-linked salt **2** exhibits a pronounced face-to-face intramolecular cation– $\pi$  interaction, reflected by a significantly shorter  $R_{cc}$  value of 3.83 Å, indicative of a stronger interaction. A similar face-to-face arrangement is observed for the anthracene-linked compound **3**; however, in this case the centroid–centroid distance is considerably longer ( $R_{cc} = 5.59$  Å). This arrangement arises from

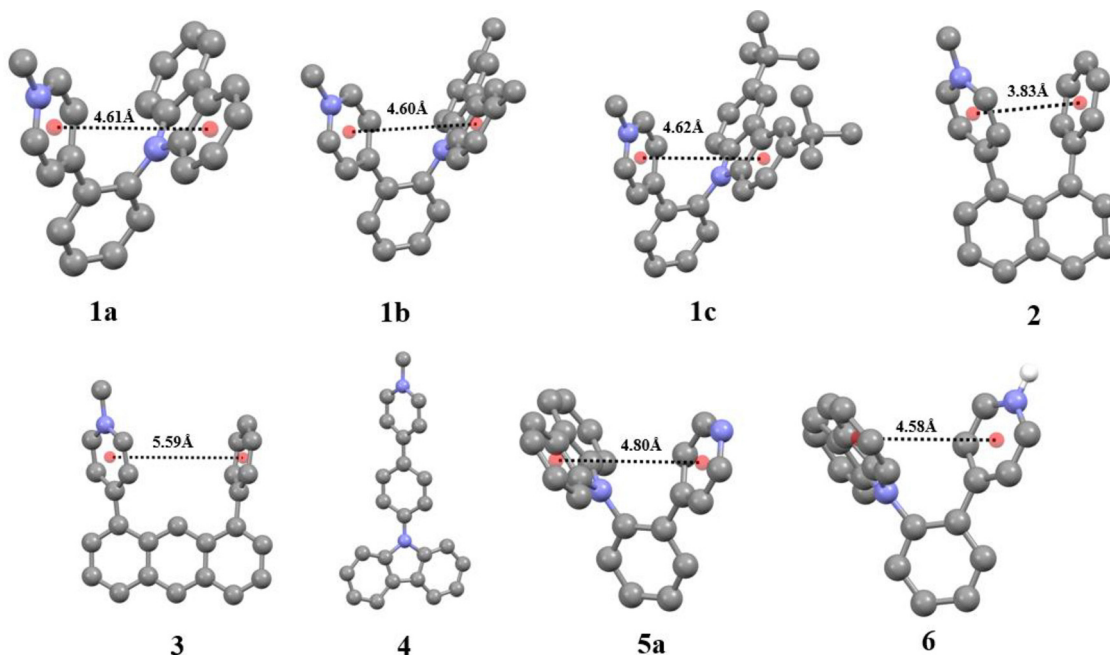


Fig. 3 Calculated geometries of **1–6** and intramolecular interaction distances.



steric repulsion between the Py<sup>+</sup> and phenyl moieties and the hydrogen atom at position 9 of the anthracene scaffold. As expected, the linear compound **4** does not permit intramolecular through-space interactions. Compound **5a**, on the other hand, displays an angled intramolecular  $\pi$ - $\pi$  interaction between the pyridine and carbazole  $\pi$ -systems, with an  $R_{cc}$  value of 4.80 Å. Given that cation- $\pi$  interactions contribute significant stabilization energies at distances of up to approximately 7 Å,<sup>26</sup> the calculated geometries of compounds **1a-c**, **2**, **3**, and **6** are consistent with the presence of intramolecular cation- $\pi$  interactions. Among these, compounds **2** and **6** exhibit the most favorable geometrical parameters and are therefore expected to display the strongest cation- $\pi$  interactions. In contrast, interactions between neutral  $\pi$ -systems are generally considered effective only within a cut-off distance of  $\sim 5$  Å;<sup>27</sup> thus, the  $\pi$ - $\pi$  interaction observed in **5a** can be classified as weak.

The NLO properties of **1-6** solutions (0.2–1.1 wt% in MeCN) were evaluated using the Z-scan technique (see Pages S12 and S13, SI). The Z-scan measurements were carried out with 150 fs laser pulse to limit the thermal contribution to nonlinear refractive index. Open-aperture (OA) measurements were used to determine NLO absorption, while closed-aperture (CA) measurements were employed to assess third- and fifth-order NLO refractive index. For fifth-order NLO measurements, third-order contributions were accounted for using a published model.<sup>28</sup> The reference Z-scan CA measurement (800 nm, pure MeCN) gave a Kerr coefficient of  $n_2 = (5.58 \pm 0.89) \times 10^{-20} \text{ m}^2 \text{ W}^{-1}$  (Fig. 4A), which is typically several orders of magnitude lower than those of PONLOMs, with no significant NLO absorption in the OA regime. The CA measurements for compounds with type **IV** designs (**1-3** and **6**) exhibited unusual NLO response, corresponding to fifth-order rather than third-order effects. For example, the Z-scan measurement of **2** (0.2 wt% in MeCN, Fig. 4B) exhibited pure negative fifth-order refraction (Fig. 4C), after the solvent (MeCN) contribution was accounted for. Further evidence for the fifth-order effect was provided by Z-scan form theory, showing a narrower peak-valley distance than that of third-order effects.<sup>29</sup> In addition, power-dependent measurements (at 800 nm; 500 kHz pulse repetition rate) were performed to analyze the NLO response (Fig. S6, SI), using the phase change parameter ( $\Phi$ ) versus laser power for pure MeCN and **2**. While  $\Phi$  varied linearly with power for MeCN, a quadratic dependence was observed for **2**, providing strong evidence

for a fifth-order effect. The pure fifth-order refraction response for **1b**, **1c**, **2**, **3**, and **6** persists up to 900 nm (Fig. S7, SI).<sup>30</sup> The Z-scan measurement examples for **1b**, **1c**, **3**, and **6** are available in the SI (see Table S2).

The fifth-order NLO efficiencies of compounds **1-6** were evaluated at 800 nm to assess their potential for photonic applications within the first telecommunication window (800–900 nm). In the case of **5a** two measurement sets were carried out, for the free base and protonated version **6** (by adding a drop of 5% aqueous HCl to MeCN). Compounds of type **IV** design (**1b**, **1c**, **2**, **3**, and **6**) exhibited a pure fifth-order NLO response with varying magnitudes. The fifth-order refractive nonlinear coefficient ( $n_4$ ) ranged from  $-877.1 \times 10^{-27}$  for salt **2** to  $-21.7 \times 10^{-27}$  for **1c** (Table 1). In contrast, **1a** displayed an extremely weak NLO response, with no detectable fifth-order component, attributable to a weak Kerr effect ( $n_2 = -0.32 \times 10^{-14}$ ). The control compounds **4** and **5a**, which lacked the intramolecular QP-MP interaction, exhibited moderate Kerr responses ( $n_2 = -2.37 \times 10^{-14}$  and  $1.78 \times 10^{-14}$ , respectively) without measurable fifth-order NLO contribution. These findings demonstrate that the type **IV** molecular design selectively suppresses the third-order Kerr effect, enabling direct access to fifth-order NLO refraction with enhanced response intensity compared to standards and other known PONLOMs.<sup>25,31</sup> This effect is particularly pronounced in compounds exhibiting the strongest intramolecular cation- $\pi$  (QP-MP) interactions, such as **2** and **6**.

The origin of the fifth-order nonlinear refraction was further examined using low repetition rate (5 kHz) and polarization-resolved Z-scan measurements. At 5 kHz, the  $n_4$  values

Table 1 Third- and fifth-order NLO coefficients,  $R_{cc}$  and  $\varepsilon$  of **1-6**

Compound	$n_2, 10^{-14} \text{ cm}^2 \text{ W}^{-1}$	$\alpha_2, 10^{-9} \text{ cm W}^{-1}$	$n_4, 10^{-26} \text{ cm}^4 \text{ W}^{-2}$	$R_{cc}$ distance, Å	$\varepsilon$ ( $\pi$ - $\pi^+$ ), $\text{M}^{-1} \text{ cm}^{-1}$
<b>1a</b>	-0.32	— <sup>a</sup>	<0.1 <sup>a</sup>	4.61	700
<b>1b</b>	— <sup>a</sup>	— <sup>a</sup>	-3.7	4.60	720
<b>1c</b>	— <sup>a</sup>	— <sup>a</sup>	-2.2	4.62	750
<b>2</b>	— <sup>a</sup>	7.6	-88.7	3.83	6670
<b>3</b>	— <sup>a</sup>	0.8	-11.0	5.59	6490
<b>4</b>	-2.37	— <sup>a</sup>	<0.1 <sup>a</sup>	n/a	—
<b>5a</b>	1.78	— <sup>a</sup>	<0.1 <sup>a</sup>	4.80	—
<b>6</b>	— <sup>a</sup>	1.0	-25.9	4.58	—

<sup>a</sup> Value below the instrument's noise threshold.

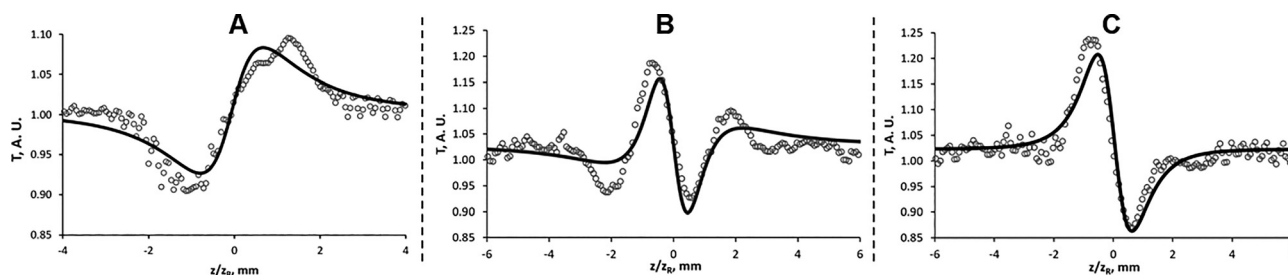


Fig. 4 Z-scan measurements at 800 nm, 500 kHz pulse repetition rate and 40.6 mW laser power. A – MeCN, B – MeCN solution of **2**, C – separated signal of **2**.



decreased to near zero for all compounds (Table S1, SI), except compound **2** ( $n_4 = -2.25 \times 10^{-26} \text{ cm}^4 \text{ W}^{-2}$  at 800 nm), indicating thermal contributions, likely associated with two-photon absorption, at higher repetition rates. However, polarization-resolved Z-scan measurements (Pages S15, S16 and Fig. S8, SI) at 500 kHz gave results that do not correspond to the thermal response. Measurements revealed a reduced phase change under circular polarization for acetonitrile ( $r = 2.03$ ) and compound **1b** ( $r = 1.49$ ). Nonlinear response dependence on polarization contradicts a pure thermal origin<sup>32</sup> that is independent from polarization and supports a dominant Kerr-type contribution for fifth-order nonlinear refraction in type **IV** molecular designs. Nevertheless, the lack of a comprehensive theoretical framework for fifth-order polarization-resolved Z-scan measurements prevents a quantitative distinction between higher-order electronic and molecular reorientation contributions.

To enable molecular-level comparison of the NLO responses, the corresponding dielectric susceptibilities and hyperpolarizabilities were calculated for all studied compounds (Table 2); the conversion equations are provided in the SI. Across the series, the calculated parameters reveal distinct dominant nonlinear mechanisms that correlate strongly with molecular design. Compounds **1a**, **4**, and **5a** are primarily governed by third-order refractive nonlinearity, as reflected by  $n_2$  and  $\chi_{\text{Re}}^{(3)}$ , with negative values for **1a** and **4** indicating self-defocusing behavior, and a positive response for **5a** consistent with enhanced through-space electronic delocalization. The negligible  $\alpha_2$  and  $n_4$  values for **1a**, **4** and **5a** indicate weak higher-order contributions. In contrast, compounds **2**, **3**, and **6** exhibit substantial nonlinear absorption ( $\alpha_2$  and  $\chi_{\text{Im}}^{(3)}$ ) together with large negative fifth-order terms ( $n_4$ ,  $\chi_{\text{Re}}^{(5)}$ , and  $\epsilon$ ). Compounds **1b** and **1c** show a suppressed third-order refractive response, but retain modest negative fifth-order parameters. Overall, these results demonstrate a clear progression from dominant third-order refraction in PONLOMs with type **I** and **III** architectures (**4** and **5a**) to a regime of attenuated third-order and enhanced fifth-order refraction response in type **IV** systems. Within the type **IV** design, strong intramolecular cation- $\pi$  (quadrupole-monopole) interactions in compounds **2**, **3**, and **6** give rise to pronounced fifth-order nonlinearity with negligible third-order refraction contributions, whereas weaker interactions in **1b** and **1c** yield only modest fifth-order effects. Notably, despite a longer interaction distance, the face-to-face geometry of compound **3** supports relatively strong cation- $\pi$  coupling, while the

angled geometry and lack of electron-donating substituents at the carbazole moiety in **1a** result in weaker interaction. Collectively, this systematic deconstruction of intramolecular interactions, from strong cation- $\pi$  to weak or absent through-space coupling, establishes that the type **IV** molecular design selectively suppresses third-order refraction while promoting dominant fifth-order nonlinear optical behavior. Notably, the type **IV** design does not indiscriminately suppress the third-order nonlinear responses, as exemplified by the presence of  $\alpha_2$  in compounds **2**, **3**, and **6** (Tables 1 and 2).

To further elucidate the origin of the observed fifth-order NLO response, the  $R_{\text{cc}}$  distances of compounds **1-3**, which share a consistent *N*-methylated pyridinium MP, were analyzed in conjunction with the molar absorption coefficients ( $\epsilon$ ) of their corresponding intramolecular  $\pi$ - $\pi^+$  CT bands (Table 1). Compounds **4** and **5a** were excluded from this analysis due to the absence of intramolecular cation- $\pi$  interactions, while compound **6** was omitted because of the unattenuated nature of its MP. The through space CT absorption in **1a-c** was relatively weak, with  $\epsilon$  values in the range of 700–750  $\text{M}^{-1} \text{ cm}^{-1}$ , whereas compounds **2** and **3** displayed significantly stronger  $\pi$ - $\pi^+$  interaction promoted absorptions, with  $\epsilon$  values of 6670 and 6490  $\text{M}^{-1} \text{ cm}^{-1}$ , respectively. Notably, an empirical correlation ( $R^2 = 0.99$ ) was observed between the fifth-order nonlinear refractive index ( $n_4$ ) and the ratio  $\epsilon/R_{\text{cc}}^4$  ( $n_4 \propto \epsilon/R_{\text{cc}}^4$ ; Fig. 5). Such a correlation indicates that the magnitude of the fifth-order NLO response is governed by the strength of the intramolecular electrostatic interaction between the neutral  $\pi$ -system and the cationic  $\pi^+$  moiety. The observed inverse

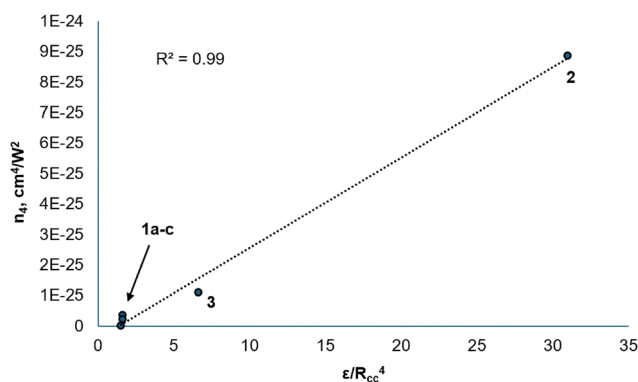


Fig. 5 Relationship between  $n_4$  and  $\epsilon/R_{\text{cc}}^4$  in compounds **1-3**.

Table 2 NLO molecular coefficients of **1-6**

Compound	$n_2, 10^{-14} \text{ cm}^2 \text{ W}^{-1}$	$\alpha_2, 10^{-9} \text{ cm W}^{-1}$	$n_4, 10^{-26} \text{ cm}^4 \text{ W}^{-2}$	$\chi_{\text{Re}}^{(3)}, 10^{-16} \text{ cm}^2 \text{ V}^{-2}$	$\chi_{\text{Im}}^{(3)}, 10^{-19} \text{ cm}^2 \text{ V}^{-2}$	$\chi_{\text{Re}}^{(5)}, 10^{-30} \text{ cm}^4 \text{ V}^{-4}$	$\gamma, 10^{-36} \text{ esu}$	$\epsilon, 10^{-48} \text{ esu}$
<b>1a</b>	-0.32	—	<0.1	-0.20	—	—	-52.42	—
<b>1b</b>	—	—	-3.7	—	—	-0.50	—	-2.6
<b>1c</b>	—	—	-2.2	—	—	-0.30	—	-1.8
<b>2</b>	—	7.6	-88.7	—	30.6	-12.0	—	-53.0
<b>3</b>	—	0.8	-11	—	3.2	-1.48	—	-7.4
<b>4</b>	-2.37	—	<0.1	-1.50	—	—	-388.21	—
<b>5a</b>	1.78	—	<0.1	1.13	—	—	214.81	—
<b>6</b>	—	1.0	-25.9	—	4.0	-3.49	—	-13.9



fourth-power dependence on  $R_{cc}$  is consistent with an MP-induced dipole interaction mechanism, in which the localized positive charge of the MP polarizes the adjacent  $\pi$ -system. This MP-induced dipole mechanism was further corroborated by DFT calculations, which show that  $n_4$  increases exponentially with the product of the MP-induced and transition dipole moments in compounds **1a**, **1b**, **1c**, **2**, and **3** (see Pages S18–S25, SI). Collectively, these results indicate an electrostatic origin for the fifth-order NLO response in type **IV** systems.

## Conclusion

In conclusion, we show that incorporating intramolecular cation– $\pi$  quadrupole–monopole (QP–MP) interactions into purely organic molecules provides a general design methodology for inverting the conventional hierarchy of nonlinear optical (NLO) responses. Structurally simple  $\pi^+$ – $\pi$  through-space conjugates within this series exhibited the ability to selectively suppress the third-order Kerr effect while producing a pure fifth-order refractive response at 800 nm. The mechanism of the fifth-order refractive response is not straightforward. Frequency-dependent measurements suggest a thermal origin, and polarization-resolved Z-scan data indicate a Kerr-type electronic contribution, pointing to a more complex origin. Notably, the naphthalene-linked derivative **2**, possessing the strongest intramolecular cation– $\pi$  (QP–MP) interaction, displayed a fifth-order response nearly three orders of magnitude greater than that of benchmark materials such as  $CS_2$ . In contrast, control molecules lacking the cation– $\pi$  (QP–MP) interaction (**4**, **5a**) showed only conventional Kerr nonlinearities, underscoring the critical role of through-space electrostatic coupling. Experimental correlations indicated that the fifth-order response scales with  $\varepsilon/R^4$ , consistent with an underlying monopole-induced dipole polarization mechanism. Hence, electrostatic through-space interactions offer a promising route to create novel multipole architectures and enable precise control of NLO properties in organic materials.

## Author contributions

The manuscript was written through contributions of all authors. Daniels Jelisejevs: investigation, methodology, and validation; Arturs Bundulis: conceptualization, investigation, methodology, validation, writing – original draft, and writing – review and editing; Anete Sapne: investigation, methodology, and validation; Kaspars Leduskrasts: conceptualization, data curation, formal analysis, investigation, methodology, validation, visualization, writing – original draft, writing – review and editing, and funding acquisition. All authors have given approval to the final version of the manuscript.

## Conflicts of interest

There are no conflicts to declare.

## Data availability

The data supporting the findings of this study are available in the supplementary information (SI). Supplementary information: detailed synthetic procedures, characterization data (including UV-vis and NMR spectra), nonlinear optical measurement methodologies, associated calculations, and the phase-change plot. See DOI: <https://doi.org/10.1039/d6tc00480f>.

## Acknowledgements

This work was funded by RRF grant no. 30/OSI/PG (RRF project no. 5.2.1.1.i.0/2/24/I/CFLA/001) and Latvian Quantum Technologies Initiative under European Union Recovery and Resilience Facility no. 2.3.1.1.i.0/1/22/I/CFLA/001. We thank Dr A. Kinens for the molecular geometry optimization and induced dipole calculations.

## References

- (a) A. Di Francescantonio, A. Zilli, D. Rocco, V. Vinel, L. Coudrat, F. Conti, P. Biagioni, L. Duò, A. Lemaître, C. De Angelis, G. Leo, M. Finazzi and M. Celebrano, All-Optical Free-Space Routing of Upconverted Light by Meta-surfaces via Nonlinear Interferometry, *Nat. Nanotechnol.*, 2023, **19**(3), 298–305, DOI: [10.1038/s41565-023-01549-2](https://doi.org/10.1038/s41565-023-01549-2); (b) D. Zhang, D. Xu, Y. Li, Y. Luo, J. Hu, J. Zhou, Y. Zhang, B. Zhou, P. Wang, X. Li, B. Bai, H. Ren, L. Wang, A. Zhang, M. Jarrahi, Y. Huang, A. Ozcan and X. Duan, Broadband Nonlinear Modulation of Incoherent Light Using a Transparent Optoelectronic Neuron Array, *Nat. Commun.*, 2024, **15**, 2433, DOI: [10.1038/s41467-024-46387-5](https://doi.org/10.1038/s41467-024-46387-5).
- (a) S. Kumar, T. Kamali, J. M. Levitte, O. Katz, B. Hermann, R. Werkmeister, B. Považay, W. Drexler, A. Unterhuber and Y. Silberberg, Single-Pulse Cars Based Multimodal Nonlinear Optical Microscope for Bioimaging, *Opt. Express*, 2015, **23**(10), 13082, DOI: [10.1364/OE.23.013082](https://doi.org/10.1364/OE.23.013082); (b) V. Parodi, E. Jacchetti, R. Osellame, G. Cerullo, D. Polli and M. T. Raimondi, Nonlinear Optical Microscopy: From Fundamentals to Applications in Live Bioimaging, *Front. Bioeng. Biotechnol.*, 2020, **8**, DOI: [10.3389/fbioe.2020.585363](https://doi.org/10.3389/fbioe.2020.585363).
- (a) L. G. Wright, W. H. Renninger, D. N. Christodoulides and F. W. Wise, Nonlinear Multimode Photonics: Nonlinear Optics with Many Degrees of Freedom, *Optica*, 2022, **9**(7), 824, DOI: [10.1364/OPTICA.461981](https://doi.org/10.1364/OPTICA.461981); (b) L. Sirleto and G. C. Righini, An Introduction to Nonlinear Integrated Photonics Devices: Nonlinear Effects and Materials, *Micro-machines*, 2023, **14**(3), 604, DOI: [10.3390/mi14030604](https://doi.org/10.3390/mi14030604).
- S. K. Turitsyn, J. E. Prilepsky, S. T. Le, S. Wahls, L. L. Frumin, M. Kamalian and S. A. Derevyanko, Nonlinear Fourier Transform for Optical Data Processing and Transmission: Advances and Perspectives, *Optica*, 2017, **4**(3), 307, DOI: [10.1364/OPTICA.4.000307](https://doi.org/10.1364/OPTICA.4.000307).
- X. Liu, X. Shen, T. Rui, L. He, B. Zhou and N. Zheng, Adiabatic Nonlinear Optical Frequency Conversion Based on the Electro-Optic Effect, *Opt. Lett.*, 2020, **45**(2), 467, DOI: [10.1364/OL.377024](https://doi.org/10.1364/OL.377024).



- 6 S. Yoon, S. Y. Cheon, S. Park, D. Lee, Y. Lee, S. Han, M. Kim and H. Koo, Recent Advances in Optical Imaging through Deep Tissue: Imaging Probes and Techniques, *Biomater. Res.*, 2022, **26**, 57, DOI: [10.1186/s40824-022-00303-4](https://doi.org/10.1186/s40824-022-00303-4).
- 7 L. Ackermann, C. Roider, K. Cvecek, N. Barré, C. Aigner and M. Schmidt, Polarization-Controlled Nonlinear Computer-Generated Holography, *Sci. Rep.*, 2023, **13**, 10338, DOI: [10.1038/s41598-023-37443-z](https://doi.org/10.1038/s41598-023-37443-z).
- 8 Y. I. Jhon, Y. M. Jhon and J. H. Lee, Nonlinear Optics of Mxene in Laser Technologies, *JPhys Mater.*, 2020, **3**(3), 032004, DOI: [10.1088/2515-7639/ab9f89](https://doi.org/10.1088/2515-7639/ab9f89).
- 9 L. Jia, J. Wu, Y. Zhang, Y. Qu, B. Jia and D. J. Moss, Third-Order Optical Nonlinearities of 2D Materials at Telecommunications Wavelengths, *Micromachines*, 2023, **14**(2), 307, DOI: [10.3390/mi14020307](https://doi.org/10.3390/mi14020307).
- 10 L. Caspani, C. Xiong, B. J. Eggleton, D. Bajoni, M. Liscidini, M. Galli, R. Morandotti and D. J. Moss, Integrated Sources of Photon Quantum States Based on Nonlinear Optics, *Light: Sci. Appl.*, 2017, **6**, e17100, DOI: [10.1038/lssa.2017.100](https://doi.org/10.1038/lssa.2017.100).
- 11 A. F. Garito, K. D. Singer and C. C. Teng, Molecular Optics: Nonlinear Optical Properties of Organic and Polymeric Crystals, *ACS Symp. Ser.*, 1983, 1–26, DOI: [10.1021/bk-1983-0233.ch001](https://doi.org/10.1021/bk-1983-0233.ch001).
- 12 (a) A. Ajami, W. Husinsky, R. Liska and N. Pucher, Two-Photon Absorption Cross Section Measurements of Various Two-Photon Initiators for Ultrashort Laser Radiation Applying the Z-Scan Technique, *J. Opt. Soc. Am. B*, 2010, **27**(11), 2290, DOI: [10.1364/JOSAB.27.002290](https://doi.org/10.1364/JOSAB.27.002290); (b) T. Tian, Y. Fang, W. Wang, M. Yang, Y. Tan, C. Xu, S. Zhang, Y. Chen, M. Xu, B. Cai and W.-Q. Wu, Durable Organic Nonlinear Optical Membranes for Thermotolerant Lightings and in Vivo Bioimaging, *Nat. Commun.*, 2023, **14**, 4429, DOI: [10.1038/s41467-023-40168-2](https://doi.org/10.1038/s41467-023-40168-2).
- 13 H. M. Kim and B. R. Cho, Small-Molecule Two-Photon Probes for Bioimaging Applications, *Chem. Rev.*, 2015, **115**(11), 5014–5055, DOI: [10.1021/cr5004425](https://doi.org/10.1021/cr5004425).
- 14 (a) M. Drobizhev, A. Karotki, A. Rebane and C. W. Spangler, Dendrimer Molecules with Record Large Two-Photon Absorption Cross Section, *Opt. Lett.*, 2001, **26**(14), 1081, DOI: [10.1364/OL.26.001081](https://doi.org/10.1364/OL.26.001081); (b) J. Wu, Z. Li, J. Luo and A. K.-Y. Jen, High-Performance Organic Second- and Third-Order Nonlinear Optical Materials for Ultrafast Information Processing, *J. Mater. Chem. C*, 2020, **8**(43), 15009–15026, DOI: [10.1039/D0TC03224G](https://doi.org/10.1039/D0TC03224G).
- 15 (a) M. S. Kodikara, R. Stranger and M. G. Humphrey, Computational Studies of the Nonlinear Optical Properties of Organometallic Complexes, *Coord. Chem. Rev.*, 2018, **375**, 389–409, DOI: [10.1016/j.ccr.2018.02.007](https://doi.org/10.1016/j.ccr.2018.02.007); (b) J. J. Wolff and R. Wortmann, Organic Materials for Second-Order Nonlinear Optics, *Adv. Phys. Org. Chem.*, 1999, 121–217, DOI: [10.1016/S0065-3160\(08\)60007-6](https://doi.org/10.1016/S0065-3160(08)60007-6).
- 16 G. P. Bartholomew, I. Ledoux, S. Mukamel, G. C. Bazan and J. Zyss, Three-Dimensional Nonlinear Optical Chromophores Based on through-Space Delocalization, *J. Am. Chem. Soc.*, 2002, **124**(45), 13480–13485, DOI: [10.1021/ja0272179](https://doi.org/10.1021/ja0272179).
- 17 J.-T. Ye and Y.-Q. Qiu, The Inspiration and Challenge for Through-Space Charge Transfer Architecture: From Thermally Activated Delayed Fluorescence to Non-Linear Optical Properties, *Phys. Chem. Chem. Phys.*, 2021, **23**(30), 15881–15898, DOI: [10.1039/D1CP02565A](https://doi.org/10.1039/D1CP02565A).
- 18 B. Gu, C. Zhao, A. Baev, K.-T. Yong, S. Wen and P. N. Prasad, Molecular Nonlinear Optics: Recent Advances and Applications, *Adv. Opt. Photonics*, 2016, **8**(2), 328, DOI: [10.1364/AOP.8.000328](https://doi.org/10.1364/AOP.8.000328).
- 19 (a) S. Roy, S. K. Nandi, D. Haldar and B. Pal, Effect of Spatial Folding of Molecules on Two-Photon Absorption and Non-linear Refraction in Foldamers, *J. Mater. Chem. C*, 2022, **10**(22), 8767–8775, DOI: [10.1039/D2TC00951J](https://doi.org/10.1039/D2TC00951J); (b) A. Chatterjee, J. Chatterjee, S. Sappati, R. Tanwar, M. D. Ambhore, H. Arfin, R. M. Umesh, M. Lahiri, P. Mandal and P. Hazra, Engineering TADF, Mechanochromism, and Second Harmonic up-Conversion Properties in Regioisomeric Substitution Space, *Chem. Sci.*, 2023, **14**(47), 13832–13841, DOI: [10.1039/d3sc04280d](https://doi.org/10.1039/d3sc04280d); (c) J. Zyss, I. Ledoux, S. Volkov, V. Chernyak, S. Mukamel, G. P. Bartholomew and G. C. Bazan, Through-Space Charge Transfer and Nonlinear Optical Properties of Substituted Paracyclophane, *J. Am. Chem. Soc.*, 2000, **122**(48), 11956–11962, DOI: [10.1021/ja0022526](https://doi.org/10.1021/ja0022526).
- 20 A. Zagata, K. Traskovskis, S. Belyakov, I. Mihailovs, A. Bundulis and M. Rutkis, Dicyanomethylene-Functionalized S-Indacene-Based D- $\pi$ -A- $\Pi$ -D Dyes Exhibiting Large near-Infrared Two-Photon Absorption Cross-Section, *Dyes Pigm.*, 2023, **208**, 110864, DOI: [10.1016/j.dyepig.2022.110864](https://doi.org/10.1016/j.dyepig.2022.110864).
- 21 K. Leduskrasts, A. Kinens and E. Suna, The Emission Efficiency of Cationic Solid State Luminophores Is Directly Proportional to the Intermolecular Charge Transfer Intensity, *Chem. Commun.*, 2023, **59**(45), 6905–6908, DOI: [10.1039/d3cc01674a](https://doi.org/10.1039/d3cc01674a).
- 22 K. Leduskrasts and E. Suna, Aggregation Induced Emission by Pyridinium–Pyridinium Interactions, *RSC Adv.*, 2019, **9**(1), 460–465, DOI: [10.1039/C8RA08771G](https://doi.org/10.1039/C8RA08771G).
- 23 (a) K. Leduskrasts, A. Kinens and E. Suna, Cation- $\pi$  Interactions Secure Aggregation Induced Emission of Planar Organic Luminophores, *Chem. Commun.*, 2019, **55**(84), 12663–12666, DOI: [10.1039/C9CC06829E](https://doi.org/10.1039/C9CC06829E); (b) K. Leduskrasts and E. Suna, Aggregation Induced Emission in One Easy Step: Pyridinium AIEgens and Counter Ion Effect, *RSC Adv.*, 2020, **10**(62), 38107–38113, DOI: [10.1039/D0RA07137D](https://doi.org/10.1039/D0RA07137D); (c) K. Leduskrasts and E. Suna, Intermolecular Charge-transfer Luminescence by Self-assembly of Pyridinium Luminophores in Solutions, *ChemistryOpen*, 2021, **10**(10), 1081–1086, DOI: [10.1002/open.202100191](https://doi.org/10.1002/open.202100191).
- 24 S. Yamada, Cation- $\pi$  Interactions in Organic Synthesis, *Chem. Rev.*, 2018, **118**(23), 11353–11432, DOI: [10.1021/acs.chemrev.8b00377](https://doi.org/10.1021/acs.chemrev.8b00377).
- 25 D. G. Kong, Q. Chang, H. Ye, Y. C. Gao, Y. X. Wang, X. R. Zhang, K. Yang, W. Z. Wu and Y. L. Song, The Fifth-Order Nonlinearity of CS<sub>2</sub>, *J. Phys. B: At., Mol. Opt. Phys.*, 2009, **42**(6), 065401, DOI: [10.1088/0953-4075/42/6/065401](https://doi.org/10.1088/0953-4075/42/6/065401).
- 26 M. S. Marshall, R. P. Steele, K. S. Thanthirawatte and C. D. Sherrill, Potential Energy Curves for Cation- $\pi$  Interactions: Off-Axis Configurations Are Also Attractive, *J. Phys.*



- Chem. A*, 2009, **113**(48), 13628–13632, DOI: [10.1021/jp906086x](https://doi.org/10.1021/jp906086x).
- 27 R. Calinsky and Y. Levy, Aromatic Residues in Proteins: Re-Evaluating the Geometry and Energetics of  $\pi$ - $\pi$ , Cation- $\pi$ , and CH- $\pi$  Interactions, *J. Phys. Chem. B*, 2024, **128**, 8687–8700, DOI: [10.1021/acs.jpcc.4c04774](https://doi.org/10.1021/acs.jpcc.4c04774).
- 28 B. Gu, J. Chen, Y.-X. Fan, J. Ding and H.-T. Wang, Theory of Gaussian beam Z scan with simultaneous third- and fifth-order nonlinear refraction based on a Gaussian decomposition method, *J. Opt. Soc. Am. B*, 2005, **22**, 2651–2659, DOI: [10.1364/JOSAB.22.002651](https://doi.org/10.1364/JOSAB.22.002651).
- 29 M. Falconieri, Thermo-Optical Effects in Z-Scan Measurements Using High-Repetition-Rate Lasers, *J. Opt. A: Pure Appl. Opt.*, 1999, **1**, 662–667, DOI: [10.1088/1464-4258/1/6/302](https://doi.org/10.1088/1464-4258/1/6/302).
- 30 A. Bundulis, K. Leduskrasts and A. Sapne, *RSC Adv.*, 2025, **15**, 48109–48115, DOI: [10.1039/D5RA07294H](https://doi.org/10.1039/D5RA07294H).
- 31 N. J. Brito e Silva, F. das Chagas de Melo Brito, H. T. M. C. M. Baltar, J. L. Magalhães, V. G. Viana, F. E. Santos and H. A. Garcia, Third- and Fifth-Order Optical Nonlinearities of Norbixin, *Results Optics*, 2022, **6**, 100205, DOI: [10.1016/j.rio.2021.100205](https://doi.org/10.1016/j.rio.2021.100205).
- 32 (a) X.-Q. Yan, Z.-B. Liu, X.-L. Zhang, W.-Y. Zhou and J.-G. Tian, Polarization dependence of Z-Scan Measurement: theory and experiment, *Opt. Express*, 2009, **17**(8), 6397, DOI: [10.1364/oe.17.006397](https://doi.org/10.1364/oe.17.006397); (b) A. Bundulis, I. Mihailovs and M. Rutkis, Origin of the kerr effect: investigation of solutions by polarization-dependent Z-scan, *J. Opt. Soc. Am. B*, 2020, **37**(6), 1806, DOI: [10.1364/josab.389520](https://doi.org/10.1364/josab.389520); (c) R. M. Moysés, E. C. Barbano and L. Misoguti, Discrimination of thermal, molecular orientation, and pure electronic refractive nonlinearities using the polarization-resolved Z-scan technique, *J. Opt. Soc. Am. B*, 2023, **40**(4), C60–C66, DOI: [10.1364/josab.482486](https://doi.org/10.1364/josab.482486).

